Received: 26 October 2021 | Revised: 6 January 2022 | Accepted: 1 March 2022

DOI: 10.1002/jbm.a.37381

RESEARCH ARTICLE

Photocurable antimicrobial silk-based hydrogels for corneal repair

Inês A. Barroso | Kenny Man | Thomas J. Hall | Thomas E. Robinson | Sophie E. T. Louth | Sophie C. Cox | Anita K. Ghag

School of Chemical Engineering, University of Birmingham, Birmingham, UK

Correspondence
Anita K. Ghag, School of Chemical Engineering, University of Birmingham, Edgbaston B15 2TT, Birmingham, UK.
Email: a.k.ghag@bham.ac.uk

Abstract

Corneal transplantation is the current gold standard treatment to restore visual acuity to patients with severe corneal diseases and injuries. Due to severe donor tissue shortage, efforts to develop a corneal equivalent have been made but the challenge remains unmet. Another issue of concern in ocular surgery is the difficult instillation and fast drainage of antibiotic ocular eye drops as bacterial infections can jeopardize implant success by delaying or impairing tissue healing. In this study, we developed antimicrobial silk-based hydrogels that have the potential to be photoactivated in situ, fully adapting to the corneal injury shape. Gentamicin-loaded methacrylated-silk (SilkMA) hydrogels were prepared within minutes using low UV intensity (3 mW/cm^2). SilkMA gels provided a Young's modulus between 21 and 79 kPa together with a light transmittance spectrum and water content (83%–90%) similar to the human cornea. Polymer concentration (15%–25%) was found to offer a tool for tailoring the physical properties of the hydrogels. We confirmed that the methacrylation did not affect the material's in vitro degradation and biocompatibility by observing fibroblast adhesion and proliferation. Importantly, agar diffusion tests showed that the synthesized hydrogels were able to inhibit *Staphylococcus aureus* and *Pseudomonas aeruginosa* growth for 72 h. These characteristics along with their injectability and viscoelasticity demonstrate the potential of SilkMA hydrogels to be applied in several soft tissue engineering fields. As such, for the first time we demonstrate the potential of photocurable antimicrobial SilkMA hydrogels as a novel biomaterial to facilitate corneal regeneration.

KEYWORDS
antimicrobial, cornea, regenerative medicine, silk fibroin

1 | INTRODUCTION

The cornea is a transparent avascular tissue located on the outermost surface of the eye. It is responsible for the protection of the inner ocular structures against trauma and infections, while playing a pivotal role in light transmission and focusing (80% of the eye refractive power).[1–3] Corneal diseases and injuries can lead to corneal thinning and opacification, eventually leading to blindness. Currently, corneal blindness is estimated to affect 23 million people worldwide, with less than 1.5% of patients benefiting from a corneal transplant due to severe tissue shortage.[2,4] Although imposing risks of donor driven

[Corrections updated on 17th Mar 2022; after first online publication. The word "methacrylic anhydride side groups" has been changed to "methacrylate side groups".]

infection and rejection, corneal transplantation is still the gold standard treatment to restore visual acuity to patients .[2,5,6] Fully synthetic prostheses KPro (keratoprosthese) are currently the only non-allogenic treatment approved for human use.[7] Although innovations in prosthesis design and postoperative management has improved treatment outcomes,[8] this procedure is associated with serious complications, such as glaucoma, retinal detachment and infections, while also requiring a high level of skill from the practitioner.[9] Due to the limitations of current clinical strategies, there has been extensive research focused on the use of polymeric biomaterials to replace damaged corneal tissue.[2,4] The use of injectable polymeric biomaterials such as hydrogels are favorable as they can either be administered directly to the corneal injury and crosslinked in situ using different methods[2,4,10–13] or 3D printed into complex and anatomically relevant geometries.[5,6,14,15] Upon implantation the artificial corneal substitute should act as a functional cornea nurturing tissue ingrowth and regeneration with low inflammatory host response. The engineered material should also be fully biodegradable, eliminating the need for further surgeries.[16] Challenges associated with bioengineered corneal substitutes include high optical transparency, sufficient cohesive strength to withstand the intraocular pressure (IOP) and eye movements, permeability to metabolites, and ability to prevent infections while sustaining epithelial and stromal cell-ingrowth.

Recently, efforts to develop stromal fillers and corneal substitutes have been made.[2,4,12,17] Fernandes-Cunha et al. developed collagen hydrogels cross-linked via multi-arm-PEG-N-hydroxysuccinimide (NHS). The gels were cross-linked within 5–10 min without the use of catalysts and its physical properties were modulated as function of the PEG concentration and number of arms. In vivo studies demonstrated that the hydrogels could be formed in situ without the use of sutures and were proven to support multi-layered re-epithelization.[4] Chen et al. used strain-promoted azide-alkyne cycloaddition to crosslink hyaluronate-collagen hydrogels under ambient conditions without the need for external initiators. The material showed a transmittance over 95% in the visible range. Hydrogels were crosslinked in situ without the need of sutures and remained clear on the rabbit corneal defect for 7 days supporting re-epithelization.[2] However, although these strategies do not require any external triggers or catalysts, they might not be suitable for applications that require fast cross-linking (30–120 s) or cell-encapsulation given the chemistry used.

Light-mediated hydrogel gelation has immense potential for regenerative medicine as cell-laden hydrogels can be cross-linked within minutes in mild environmental conditions. Importantly, photocurable hydrogels provide the clinician with increased flexibility in controlling in situ gelation when compared with other methods.[2,4] These photosensitive polymers have the potential to be applied as stromal fillers (in situ cross-linking)[1,3,11,12,18] or used to develop a patient-specific artificial cornea using 3D printing technologies such as lithography and extrusion-based bioprinting.[5,15,19–21] Sani et al. developed a highly biocompatible and transparent GelMA-based filler for corneal reconstruction. The hydrogels were photocured within minutes using visible light (100 mW/cm^2) and a photoinitiator solution composed of Eosin Y (photoinitiator), TEA (co-initiator), and VC (co-monomer). In vivo studies performed using a rabbit stromal defect model demonstrated the sealing efficacy of the material while allowing re-epithelization and stromal regeneration.[18]

Silk fibroin (SF)-based biomaterials have been extensively studied for numerous tissue engineering applications due to their amenability to modification, outstanding transparency, mechanical strength, and biodegradability, making it an attractive material for corneal regenerative applications.[22,23] In particular, SF membranes have been widely explored for corneal and retinal reconstruction due to their permeability and high transparency (90.6%).[24–26] However, most studies concerning SF hydrogels are based on the protein self-assembly into β-sheet-rich networks.[27] Despite providing strength to the hydrogels through physical crosslinking, these β-sheet structures decrease the optical clarity and elasticity of the gels since the crystals block long-range molecular displacements. Furthermore, the clinical application of these materials is limited due to the long gelation times and harsh environmental conditions used to induce β-sheet formation (e.g., low pH, vortexing, or methanol treatments).[27] Thus, chemically modifying SF via the addition of methacrylate side groups allows for the covalent crosslinking of SF hydrogels via photocrosslinking. This provides increased mechanical strength but also allows for greater control of the in situ cross-linking kinetics. Finally, SilkMA prepolymer solutions are injectable and liquid at room temperature which makes solution handling easier than gelatin or GelMA. Thus, there is tremendous potential of harnessing photocurable SF-based hydrogels for corneal regeneration.

Bacterial infections can cause corneal scarring and prolong or impair the wound healing process.[28,29] Therefore, the application of antibiotic eye drops and ointments is standard procedure post-surgery. However, its efficacy is limited due to fast ocular drainage and difficulties in instillation.[30] The hydrophilic nature of SF provides a solubilizing environment for antibiotics, anti-inflammatory agents, and growth factors, ultimately increasing the functionality of the medical device.[31]

In this study, we investigated the development of a photocurable antimicrobial SF hydrogel for corneal regeneration. SF was modified by methacrylation to yield a photosensitive solution that can be chemically cross-linked within minutes using UV light. As shown in Figure 1, the physical, mechanical, and biological properties of methacrylated-silk (SilkMA) hydrogels, including water content, rheology, porosity, compressive modulus, degradation, and in vitro biocompatibility were studied. Finally, the drug release profile and antimicrobial properties of gentamicin-loaded SilkMA were assessed. The development of a semi-synthetic silk-based hydrogel has potential to be applied in ocular surface reconstruction due to its viscoelasticity, cytocompatibility, and antimicrobial properties.

2 | METHODS

2.1 | Silk fibroin extraction

Bombyx Mori cocoons were supplied by The Yarn Tree (Roanoke). Each cocoon was sliced into four pieces and the silkworms were

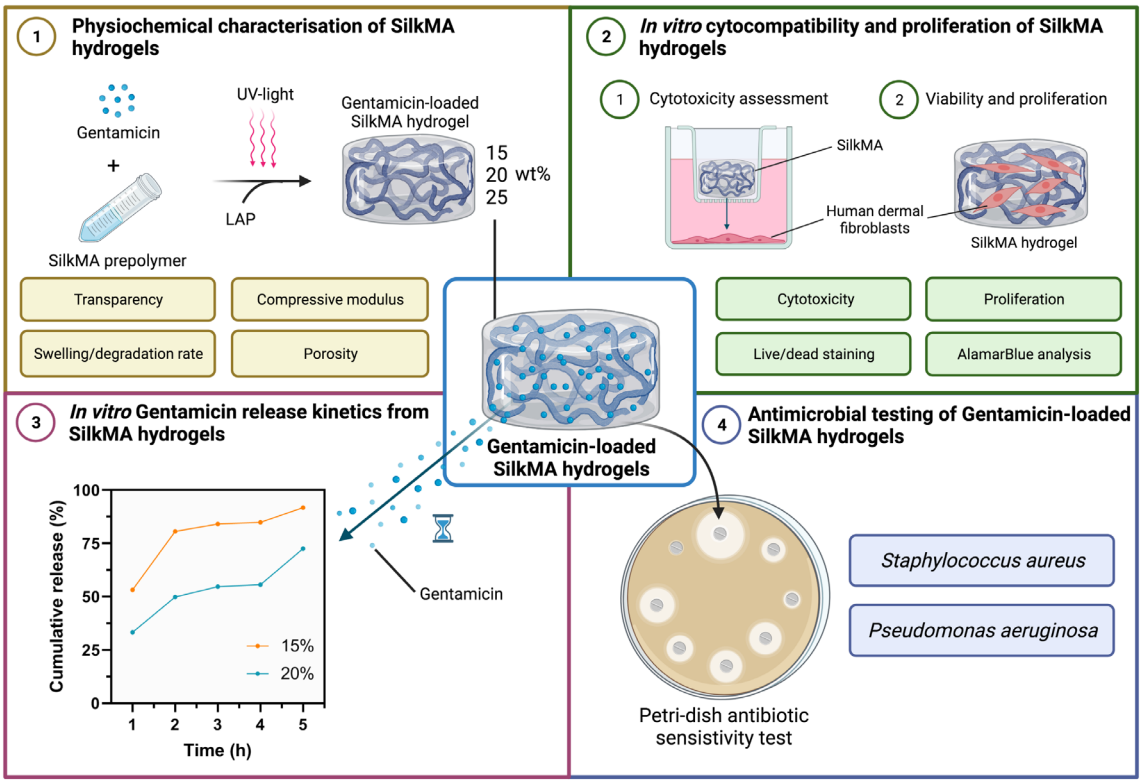

FIGURE 1 Experimental outline investigating the properties of gentamicin-loaded SilkMA hydrogels. (1) Photocrosslinking of 15%, 20%, and 25% gentamicin-loaded SilkMA hydrogels. The transparency in the visible range, swelling, in vitro degradation, porosity/pore size, compressive Young's modulus, and rheological properties of the SilkMA hydrogels were studied. (2) In vitro cytocompatibility of gentamicin-loaded SilkMA hydrogels. Firstly, the cytocompatibility of SF and SilkMA prepolymer solutions and SilkMA hydrogels was assessed. Then, the ability of human dermal fibroblast (HDF) cells to attach and proliferate on SilkMA hydrogels was studied and compared with GelMA hydrogels. (3) In vitro gentamicin drug release from SilkMA hydrogels. The cumulative drug release of gentamicin from SilkMA hydrogels and gentamicin concentration in the media were calculated. (4) Antimicrobial testing of gentamicin-SilkMA hydrogels. The antimicrobial activity of SilkMA hydrogels against two of the most common causes of ocular infections, *Staphylococcus aureus* and *Pseudomonas aeruginosa* was assessed in vitro

discarded. To remove the sericin, 10 g of sliced cocoons were boiled in 4 L of 0.02 M Na_2SO_3 (Acros Organics, Belgium) for 30 min. Subsequently, the degummed silk fibroin (SF) was washed three times in 2 L of distilled water for 20 min and left in a fume hood overnight to dry at room temperature.

2.2 | SilkMA synthesis

Briefly, 25% (wt/vol) of degummed SF solution was prepared by pouring a 9.3 M lithium bromide (LiBr) solution (Acros Organics, Belgium) on the tightly packed degummed silk fibroin fibers. After incubation at 60°C for 1 h, the fibers were completely dissolved and glycidyl methacrylate (GMA) (Sigma-Aldrich) was added to the solution (10% vol/vol) and allowed to react for 3 h at 60°C with a stirring speed of 300 rpm. The solution was then dialyzed against distilled water for 7 days at 4°C using 12–14 kDa cut-off dialysis tubes (Thermo Scientific). After dialysis, the SilkMA solution was diluted to 2% (wt/vol), and the pH adjusted to 7.4 using 1 mM sodium hydroxide solution (Sigma-Aldrich). Lastly, SilkMA solutions were lyophilized for 2 days to generate a white porous foam, which was stored at −80°C until further use.

2.3 | Degree of methacrylation

The degree of methacrylation (DM%) was quantified by proton nuclear magnetic resonance (^{1}H-NMR). Briefly, 5 mg of SilkMA were dissolved in 600 μl deuterium oxide (Sigma-Aldrich). The ^{1}H-NMR spectra of raw SF and SilkMA were recorded using a Bruker NEO NMR spectrometer fitted with a "smart"-BBFO probe (Bruker, Austria) operating at 400 MHz for 1 h. Spectra were recorded at 25°C using 250 scans and a delay of 12 s between scans. Baseline and phase correction were applied before integrating the peaks of interest with Topspin software (Bruker, Austria). The signal from the aromatic amino acids (6.9–7.5 ppm) was used as the internal reference to normalize the amine signals (2.83–3.14 ppm).[19] As GMA reacts with SF through the primary amines on lysine residues, the extent of substitution was calculated by normalization to the number of free amino groups of original SF. The degree of methacrylation was calculated using the following equation:

$$\mathrm{DM}\,(\%) = \frac{\text{lysine integration signal of SilkMA}}{\text{lysine integration signal of SF}} \times 100 \quad (1)$$

2.4 | Preparation of gentamicin-loaded SilkMA gels

In this work, three different formulations were tested: 15%, 20%, and 25% (wt/vol) SilkMA gels loaded with 0.2% (wt/vol) gentamicin sulphate (G-Biosciences). Briefly, 15%, 20%, and 25% SilkMA solutions were prepared by dissolving an appropriate amount of SilkMA in phosphate-buffered saline (PBS, pH 7.4) (Sigma-Aldrich, UK) at room temperature overnight. The resulting viscous solutions were filtrated using Miracloth (Merck Millipore). A fresh stock solution of 2% (wt/vol) lithium phenyl-2,4,6-trimethylbenzoylphospinate (LAP) (Sigma-Aldrich, UK) in PBS was prepared. The photoinitiator was added to the SilkMA solution to a final concentration of 0.5% (wt/vol) and the resulting solution was mixed at room temperature. The hydrogel precursor solutions were photocured through UV-light using an OmniCure S1500 (Lumen Dynamics, Ontario, Canada) with a 365 nm filter. Briefly, 200 μl of SilkMA prepolymer solution was pipetted onto a 12 mm cylindrical mold and then exposed to 3 mW/cm^2 of UV-A for 5 min.

2.5 | Transparency

Light absorbance of hydrogels in the visible range (400–800 nm) was measured using a microplate reader (Spark Multimode, Tecan, Switzerland). The measurements were carried out in triplicate using SilkMA hydrogels (radius = 6 mm, thickness = 1.2 mm) in PBS with pure PBS serving as a blank control. Subsequently, the transmittance was calculated using Equation (2).

$$\text{Transmittance}\,(\%) = 10^{2-\text{Absorbance}} \quad (2)$$

2.6 | Swelling properties

SilkMA hydrogels with a radius of 6 mm and a thickness of 1.2 mm were prepared. Immediately after calculating the initial hydrogel weight (m_{t0}), three samples from each condition were immediately freeze-dried ($m_{t0,dry}$) and three samples were hydrated in PBS and placed in an incubator at 32°C. After 24 h, samples were blotted dry using filter paper and the swollen weight ($m_{swollen}$) was measured. Finally, the swollen hydrogels were lyophilized and weighed to determine the dry sample weight ($m_{swollen,dry}$). The sol fraction is a measurement of the macromers not crosslinked in the hydrogel network and was defined as the mass loss after 24 h.[32,33] The mass swelling ratio (q), water content (WC), and mass loss were calculated according to the following equations:

$$\text{Mass swelling ratio}\,(q) = \frac{m_{swollen}}{m_{t0,dry}} \quad (3)$$

$$\text{Water content}\,(\%) = \frac{m_{swollen} - m_{t0,dry}}{m_{swollen}} \times 100 \quad (4)$$

$$\text{Mass loss}\,(\%) = \frac{m_{t0,dry} - m_{swollen,dry}}{m_{t0,dry}} \times 100 \quad (5)$$

The thickness of the fresh and swollen hydrogels was estimated using ImageJ software (version 2.0) and the expansion (%) in PBS after 24 h calculated. Tests were performed in triplicate.

2.7 | Rheological characterization

The storage modulus (G′) and loss modulus (G″) of freshly prepared hydrogels were measured in oscillatory mode. A frequency sweep was conducted between 0.01 and 10 Hz at 0.5% shear strain at 32°C using a plate-plate geometry (Kinexus Pro+, Malvern, UK). The experiments were conducted in triplicate. The damping factor (tan δ) was calculated using the following equation:

$$\tan\delta = \frac{G''}{G'} \quad (6)$$

2.8 | Enzymatic degradation

Disc-shaped hydrogels (radius = 3 mm, thickness = 2 mm) were prepared as previously described. After photocrosslinking, five samples of each group were immediately freeze-dried to calculate the initial weight. To determine the in vitro degradation, five samples of each group were placed in 1.5 ml tubes with 1 ml of 1 U/ml collagenase II in PBS (Fisher Scientific, UK) or in 1 ml PBS (control group) and incubated at 32°C for 2, 5, and 7 days. At the end of the incubation period the hydrogels were lyophilized. The degradation was calculated using the following equation:

$$\text{Degradation}\,(\%) = \frac{m_{t0,dry} - m_{dry}}{m_{dry}} \times 100 \quad (7)$$

Where $m_{t0,dry}$ is the initial dry weight of the hydrogels and m_{dry} is the final dry weight of the sample after degradation ($n = 5$).

2.9 | Micro-computed tomography

Freeze-dried hydrogels were scanned using the Skyscan 1172 (Bruker, Germany) with 80 kV beam voltage and 100 μA current, 140 ms exposure per projection, 12.99 μm pixel size, rotation step 0.6° and 4 frame averaging. The same parameters were used for all scans. 2D projections were reconstructed and visualized using

NRecon (Version 1.6.10, Bruker) and CTVox (Version 3.0, Bruker), respectively. Further numerical analysis was performed in CTAn (Bruker).

2.10 | Scanning electron microscopy

Scanning electron microscopy (SEM) was used to assess the morphology and pore size of freeze-dried hydrogels. All samples (diameter = 6 mm, thickness = 2 mm) were mounted onto aluminum stubs using carbon tape and gold sputter coated. Images were captured using a TM3030Plus benchtop SEM (Hitachi High Technologies, Schaumburg) at an electron acceleration voltage of 15 kV.

2.11 | Mechanical characterization

Cyclic testing was performed using an Instron 5542 mechanical tester (Instron) with a 2 kN load cell. Cylindrical hydrogels (radius = 4 mm, thickness = 2 mm) were prepared as previously described and incubated in PBS for 4 h prior to testing. The dimensions of the samples were determined using a digital caliper. Compressive tests were performed at a rate of 1 mm/min up to a maximum strain of 60% of the original height by performing 8 cycles of loading and unloading. The compressive strain (mm) and load (N) was recorded using Bluehill 3 software. The Young's modulus was calculated from the slope of the linear region on the stress (kPa) versus strain (mm/mm) curves. Samples were tested in triplicate for each condition.

2.12 | In vitro cytocompatibility of SilkMA hydrogels

Human Dermal Fibroblasts (HDFs—ATCC Cat. PCS-201-012; Passage number 9) were cultured in Dulbecco's modified eagle medium (DMEM—Sigma-Aldrich, UK) and supplemented with 10% fetal bovine serum (Sigma-Aldrich, UK), 1% penicillin/streptomycin (Sigma-Aldrich, UK) and 2 mM L-glutamine (Sigma-Aldrich, UK). All cultures were maintained in tissue culture treated polystyrene flasks at 37°C with 5% CO_2 in a humidified incubator and passaged at 80% confluency.

2.12.1 | Cell viability

Fifteen percent SF and SilkMA pre-polymer solutions and SilkMA hydrogels were UV-sterilized for 20 min prior to use. Tissue culture treated 24-well plates (Corning, UK) were initially seeded with HDFs (1×10^4 cells/well). After 24 h, 100 μl of each sample was added to 24 well ThinCert cell culture inserts (Greiner Bio-One, UK) with 0.4 μm pore size. The monolayer cultures were incubated at 37°C with 5% CO_2 in a humidified incubator. Cell viability was evaluated using a Live/Dead assay (Thermo Fisher, UK) according to the manufacturer's instructions. Briefly, SYTO 10 green fluorescent nucleic acid stain (2 μl/ml) and ethidium homodimer-2 nucleic acid stain (2 μl/ml) were diluted in PBS to form the staining solution. At each time point, cell medium was removed, and samples were incubated with the staining solution for 15 min in the dark at 37°C. The staining solution was removed, and the samples were washed twice with PBS. The monolayer cultures were imaged with a fluorescent microscope (EVOS M5000, Thermo Fisher, UK) at days 1 and 3.

2.12.2 | 2D cell seeding on SilkMA gels

Fifteen percent SilkMA pre-polymer solutions were prepared as previously described and gelatin methacryloyl (GelMA - type A, bloom 300) was used as the control. Briefly, 15% (wt/vol) GelMA pre-polymer solution was prepared by dissolving an appropriate amount of polymer in PBS at 37°C for 30 min. Then, LAP was added to the GelMA solution to a final concentration of 0.5% (wt/vol) and the resulting solution was mixed at 37°C. SilkMA and GelMA pre-polymer solutions were UV-sterilized and photocrosslinked as described above in 48-well suspension cell culture plates (Sarstedt, UK). After curing, the hydrogels were washed with sterile PBS (Sigma-Aldrich, UK) for 15 min and soaked in supplemented DMEM overnight. One hour before cell seeding, the hydrogel matrices were partially dried to potentiate cell penetration. Then, 60 μl of cell suspension was added drop-wise onto each hydrogel (9×10^3 cells per scaffold) and samples were incubated for 1 h at 37°C with 5% CO_2 to bolster cell adhesion. After 1 h, DMEM was carefully added to the wells without disturbing the cell-laden hydrogels.[34] Culture medium was changed every 2 days.

2.12.3 | 2D cell metabolic activity

AlamarBlue™ assay (Thermo Fisher, UK) was used to determinate the relative metabolic activity according to the manufacturer's protocol. Briefly, the samples were incubated with 0.5 ml of 10% alamarBlue™ reagent in culture medium for 4 h at 37°C with 5% CO_2. Thereafter, 50 μl of cell culture medium were transferred to a 96-well plate (Corning, UK) and the fluorescence intensity was measured with a microplate reader (Spark Multimode, Tecan, Switzerland) using an excitation wavelength of 540 nm and an emission wavelength of 590 nm. Acellular hydrogels were used as a negative control and their fluorescence was subtracted from the same group seeded hydrogels to account for the background ($n \geq 4$).

2.13 | In vitro release of gentamicin from SilkMA gels

To study the in vitro drug release profile of gentamicin from SilkMA hydrogels, samples were incubated in 0.5 ml PBS in 48-well tissue-culture plates at 32°C. As prepared SilkMA hydrogels were used as blank. At each

time point, 33 μl of media was withdrawn from the well and immediately mixed with 33 μl of phthaldialdhehyde reagent (OPA, Sigma-Aldrich, UK) and 33 μl isopropanol (Sigma-Aldrich, UK) in a 96-well UV-transparent microplate (Greiner Bio-One, UK). The withdrawn samples were replaced with equal volumes of fresh PBS. Gentamicin release was measured with a microplate reader (Spark Multimode, Tecan, Switzerland) in fluorescence using an excitation wavelength of 340 nm and an emission wavelength of 430 nm. The concentration of gentamicin was extrapolated from a previously validated calibration curve and divided by the total amount of gentamicin encapsulated in the hydrogel to obtain the percentage released ($n = 5$).

2.14 | In vitro antimicrobial efficacy testing

2.14.1 | Preparation of bacterial inocula

Luria Bertani broth (Sigma-Aldrich, UK) and Luria Bertani broth with agar (Sigma-Aldrich, UK) were prepared using distilled water and at concentrations of 20 and 35 g/L, respectively. Both broth and broth with agar were then sterilized via autoclaving for 20 min at 121°C under 100 KPa of pressure (Astell, UK). Overnight cultures of *Staphylococcus aureus* (ATCC 29213) and *Pseudomonas aeruginosa* (NCTC 13437) were prepared whereby one bacterial colony was inoculated in 5 ml of LB broth. Using a Jenway 6300 UV–VIS spectrophotometer (Cole Parmer, UK) optical density measurements were taken at 600 nm for each overnight culture. Cultures were then diluted to an optical density of 0.06. Luria Bertani broth with agar was poured to form agar plates. These were then inoculated with the bacterial cultures using a hockey stick spreader.

2.14.2 | Zones of inhibition

Fifteen percent and 20% gentamicin loaded SilkMA gels prepared as previously described, were placed onto the inoculated plates and incubated at 37°C for 24 h. The zones of inhibition (ZOI) formed from inhibited bacterial growth were then measured and recorded. SilkMA gels were then transferred from the 24 h plates onto freshly inoculated agar plates, incubated for a further 24 h and with measurements taken at 48 h. This process was repeated to obtain inhibitory results after 72 h. Each SilkMA formulation and bacterial strain were run in triplicate.

2.15 | Statistical analysis

For each experiment, at least three samples were tested. One or two-way analysis of variance (ANOVA) and the Tukey test were used to determine statistically significant differences with GraphPad Prism 8.0 software. The level of significance was set at $p < .05$. Data are presented as mean value ± *SD*.

3 | RESULTS

3.1 | Physicochemical characterization of SilkMA Gels

H^1-NMR spectroscopy showed that 35%–40% of SF lysine groups were functionalized with methacrylate groups (Figure S1). Three different SilkMA hydrogel concentrations (wt/vol %) were prepared: 15%, 20%, and 25%. The optical transmittance measurements of SilkMA hydrogels in the visible range (400–800 nm) are shown in Figure 2A,B. The transparency of 15% and 20% SilkMA hydrogels was 83 ± 3% and 80 ± 1%, respectively, with both hydrogels showing high optical clarity (Figure 2C).[35] However, a negative correlation between hydrogel concentration and transmittance was observed, with 25% hydrogels having a statistically significant lower transparency (63 ± 2%) compared with 15% and 20% ($p < .001$). To determine the mass swelling ratio (q), water content and the expansion, hydrogels were incubated in PBS at the ocular temperature (32°C) for 24 h. The swelling characteristics were inversely proportional to the polymer concentration; the q of the 15, 20 and 25% gel was 9.8 ± 0.2, 8.6 ± 0.2, and 5.8 ± 0.1 respectively, with 15% and 20% ($p < .0001$) showing a significantly higher q values compared with 25% (Figure 2D). The water content results followed a similar trend, with 15% (89.8 ± 0.3%) and 20% (88.3 ± 0.4%) exhibiting significantly higher values ($p < .0001$) compared with 25% (82.7 ± 0.3%) (Figure 2E). As shown in Figure 2F, 15% SilkMA hydrogels (28.5 ± 7.1) exhibited a twofold significant higher expansion in PBS compared with 20% (14.4 ± 4.7) and 25% (14.3 ± 4.1) gels ($p < .05$).

Storage modulus (G′) and loss modulus (G″) represent the elastic and reversible response of the materials and the viscous and irreversible rearrangement of the polymeric structure of the hydrogel, respectively.[36] As shown in Figure 3A, G′ is one order of magnitude higher than G″ regardless of the SilkMA concentration, which is a typical behavior of elastomeric materials.[19] Moreover, a positive correlation between the rheological properties and polymer concentration was observed (Figure 3B,C); 25% (10.4 ± 0.2 kPa) hydrogels had a significantly higher G′ than 20% (3.0 ± 0.4 kPa, $p < .0001$) and 15% (1.1 ± 0.3 kPa, $p < .0001$) hydrogels by 3 and ninefold, respectively, while 20% hydrogels shown a threefold higher G′ than 15% gels ($p < .001$). Despite observing a nonsignificant difference in G″ between 15% and 20% SilkMA gels, G″ was proportional to the polymer concentration, ranging from 45 to 568 Pa for 15% and 25% hydrogels, respectively; 25% SilkMA hydrogels presented greater G″ than 15% ($p < .001$) and 20% (164 Pa, $p < .001$) gels by a 4 and 12-fold factor. Finally, the damping factor was lower than 0.06 for all the groups studied, suggesting a solid-like behavior (Figure 3D).[37]

The in vitro susceptibility of SilkMA gels to enzymatic degradation was studied by incubating the hydrogels in 1 U/ml collagenase II for up to 7 days. Our results show that there was a time-dependent increase in degradation, with higher polymer concentrations exhibiting lower mass loss over time. As shown in Figure 4A, no significant differences were observed between the groups after 2 and 5 days of incubation. However, at day 7, 15% SilkMA gels were completely

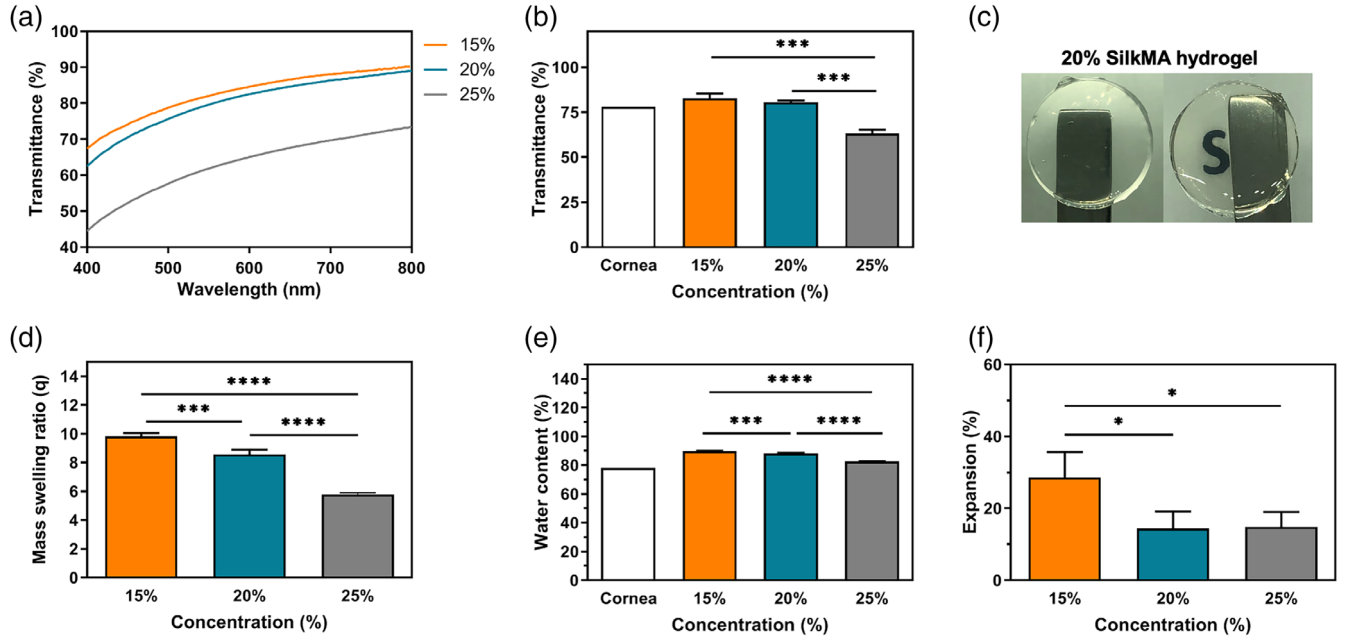

FIGURE 2 SilkMA hydrogels transparency ($n = 3$): (A) transmittance profiles, (B) average optical transmittance in the visible range, and (C) optical clarity. Hydrogel diameter = 10 mm. Swelling characteristics of SilkMA hydrogels in PBS at 32°C ($n = 3$): (D) swelling ratio (q), (E) water content (%), and (F) expansion (%). Data presented as mean value ± *SD* (*p<.0001)

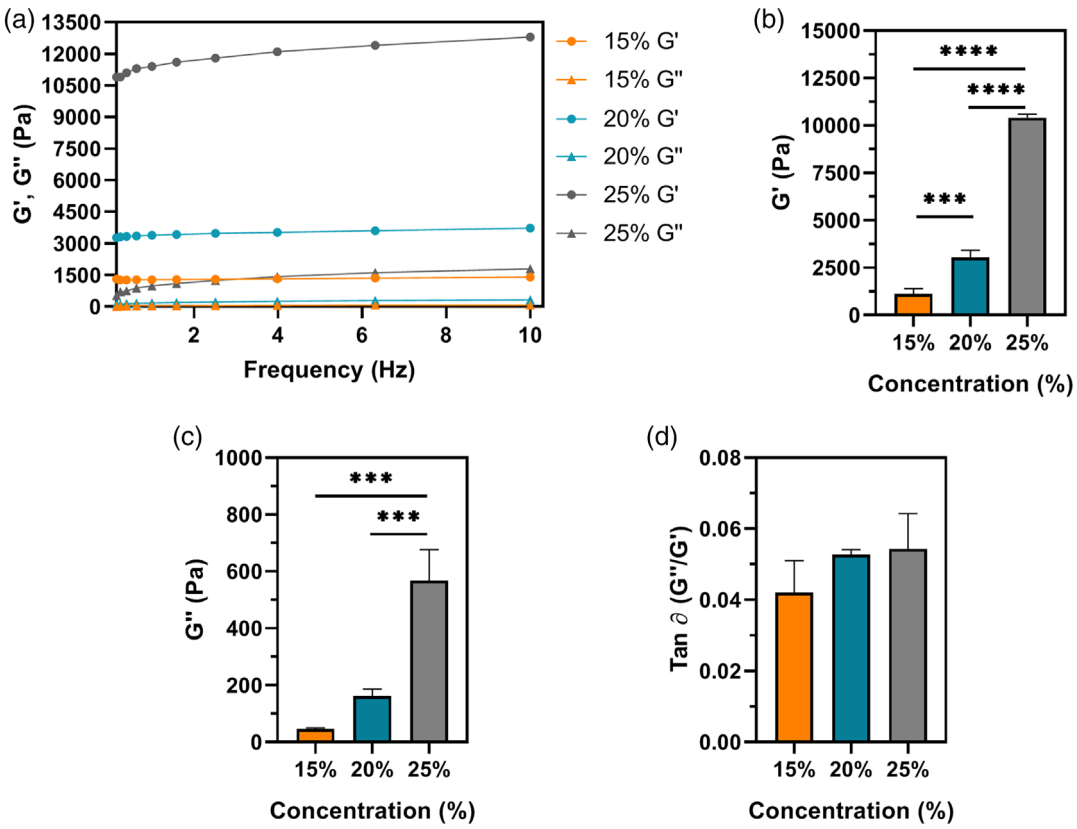

FIGURE 3 Rheological properties of SilkMA hydrogels ($n = 3$): (A) representative frequency sweep, (B) storage modulus (G′), (C) loss modulus (G″) and (D) damping factor (tan ∂). Data presented as mean value ± *SD* (*p<.05, **p<.01, ***p<.001, ****p<.0001)

degraded, while 20% and 25% SilkMA showed a degradation of 88 ± 2% and 69 ± 12% (p <.01), respectively. Due to the importance of the optical and swelling properties in the design of materials for corneal engineering, only SilkMA 15% and 20%, formulations with similar

characteristics to the human cornea, were chosen for further characterization.[38] The crosslinking efficiency was measured by mass loss, which is defined by the amount of uncrosslinked polymer after photocuring.[39] Regardless of the polymer concentration, there was no significant difference in mass loss (≃5%, Figure 4B), suggesting that the increase in concentration and viscosity did not impact the mixing between the polymer and the photoinitiator/gentamicin solution or the free radical diffusion within the material during crosslinking. Finally, the mechanical performance of the SilkMA hydrogels was assessed by compressive mechanical testing (Figure 4C). In agreement with the rheology data, 20% hydrogels showed a significantly higher Young's modulus than 15% gels (p <.0001). Specifically, the Young's modulus was 21 ± 2 kPa for 15% and 79 ± 2 kPa for 20%, a fourfold increase (Figure 4D).

The microstructure and morphology of SilkMA hydrogels were investigated using micro-CT and SEM analysis. Micro-CT scanning was used to determine the porosity, pore size and pore wall thickness within the 15% and 20% SilkMA hydrogels (Figure 5A). As shown in Figure 5B, the total porosity was 79 ± 2% and 72 ± 2% for 15 and 20% SilkMA (p <.05), respectively. However, despite the differences in porosity, the scaffolds exhibited similar pore thickness (≃26 μm, Figure 5C) and pore size distributions (Figure 5D,E), with a mean pore size of 56 ± 4 μm and 56 ± 3 μm for 15% and 20% SilkMA scaffolds, respectively (Figure 5F). SEM images revealed a uniform and interconnected pore structure for both groups (Figure 5G,H).

3.2 | In vitro assessment of cytocompatibility

The cytocompatibiliy of SF and SilkMA prepolymer solutions and SilkMA hydrogels was studied using HDF cells seeded on tissue culture well-plates. Fluorescence staining (Figure 6A) indicates high cell viability (> 90%) for all tested conditions, suggesting that SF and SilkMA materials did not induce toxicity. After 72 h, cells reached confluency for all groups studied. Furthermore, the ability of SilkMA gels to support cell attachment and proliferation was studied by direct seeding of HDF cells on SilkMA hydrogels and compared with GelMA, another semisynthetic-polymer and broadly used material for 3D cell culture applications.[40] As shown in Figure 6B, the metabolic activity progressively increased over the course of 14 days for both groups studied. The difference between the metabolic activity of HDF cells seeded on GelMA and SilkMA is only statistically significant at day 1 (p <.0001), with cells seeded on SilkMA hydrogels exhibiting a 47% lower metabolic activity. On days 2, 7, and 14, there was a 10% difference in cell metabolic activity between GelMA and SilkMA samples, however, it is not statistically significant (Figure 6B).

3.3 | In vitro drug release studies

The release kinetics of gentamicin from 15% and 20% SilkMA hydrogels was studied. As shown in Figure 7A, 15 and 20% hydrogels

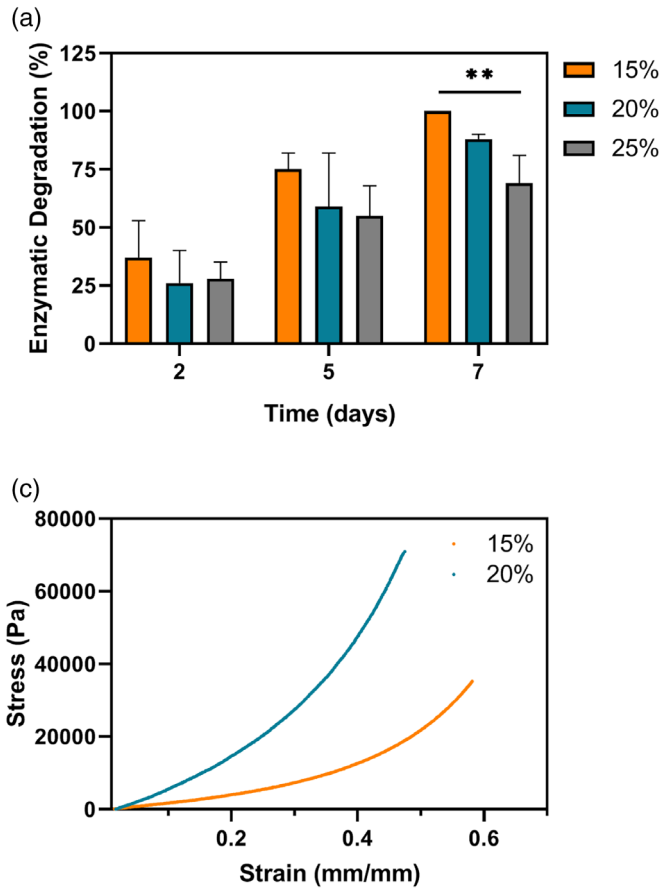

FIGURE 4 (A) In vitro degradation of SilkMA hydrogels incubated in 1 U/ml collagenase II at 32°C for 2, 5, and 7 days ($n = 5$). (B) Measurement of the macromers not crosslinked in the hydrogel network after photocrosslinking (mass loss, %) ($n = 3$). Cyclic compressive mechanical testing of SilkMA hydrogels ($n = 3$): (C) representative compressive strain-stress curves and (D) Young's moduli. Data presented as mean value ± *SD* (*p<.05, **p<.01, ***p<.001, ****p<.0001)

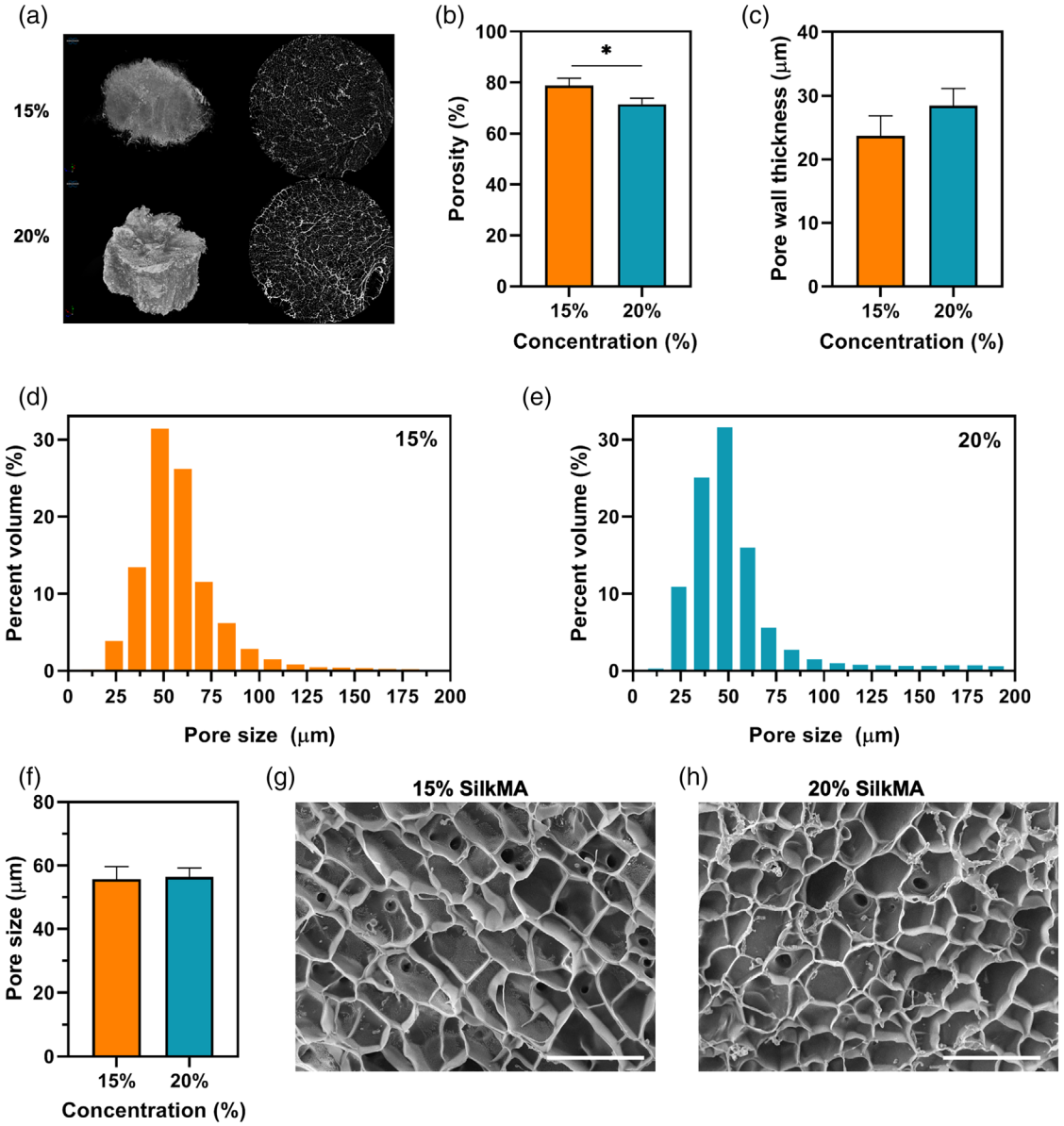

FIGURE 5 Morphology and microstructure analysis of SilkMA hydrogels after freeze drying ($n = 3$): (A) 3D micro-CT reconstruction and 2D images (slices) of SilkMA scaffolds. Diameter = 7 mm. Quantitative analysis of porosity by micro-CT: (B) total porosity, (C) mean pore thickness, (D,E) pore size distribution in the hydrogels, and (F) mean pore size. Representative SEM images of freeze-dried SilkMA scaffolds: (G) 15% SilkMA, and (H) 20% SilkMA. Scale bar: 150 μm. Data presented as mean value ± *SD* (*p<.05, **p<.01, ***p<.001, ****p<.0001)

released 53 ± 4% and 33 ± 8% (p <.02) of the total content of gentamicin within 1 h. After 2 and 5 h, 15% SilkMA gels released 84 ± 4% and 92 ± 4% (p >0.05), respectively, of the total gentamicin encapsulated, while 20% SilkMA hydrogels delivered 55 ± 4% and 72 ± 13% (p <.02), respectively. The concentration of gentamicin in the media after 24 and 48 h was determined and compared with the minimum inhibitory concentration (MIC) of gentamicin for *S.aureus* and *P. aeruginosa*. Fifteen percent and 20% SilkMA hydrogel delivered concentrations above the MIC for *S.aureus* (8 μg/ml) and *P.aeuruginosa* (2 μg/ml) after 24 and 48 h incubation.[41] As shown in Figure 7B, the concentration of gentamicin in the media was ~85 ± 6 μg/ml and 15 ± 2 μg/ml after 24 and 48 h, respectively, for both groups.

3.4 | Antimicrobial efficacy testing

Agar diffusion tests were performed to study the antimicrobial efficacy of gentamicin-loaded SilkMA gels against *S.aureus* and *P. aeruginosa*. Briefly, 15% and 20% SilkMA gels were prepared and placed on culture dishes uniformly covered with *S.aureus* or *P. aeruginosa*. After incubation at 37°C for 24 h, the zones of inhibition (ZOI) were recorded, and the same hydrogel was transferred to a freshly inoculated plate. This process was repeated until a ZOI was present. As shown in Figure 7D,E, both 15 and 20% SilkMA hydrogels inhibited the growth of *S.aureus* and *P.aeruginosa* for 72 h. However, no statistical difference was observed between the ZOI of 15 and

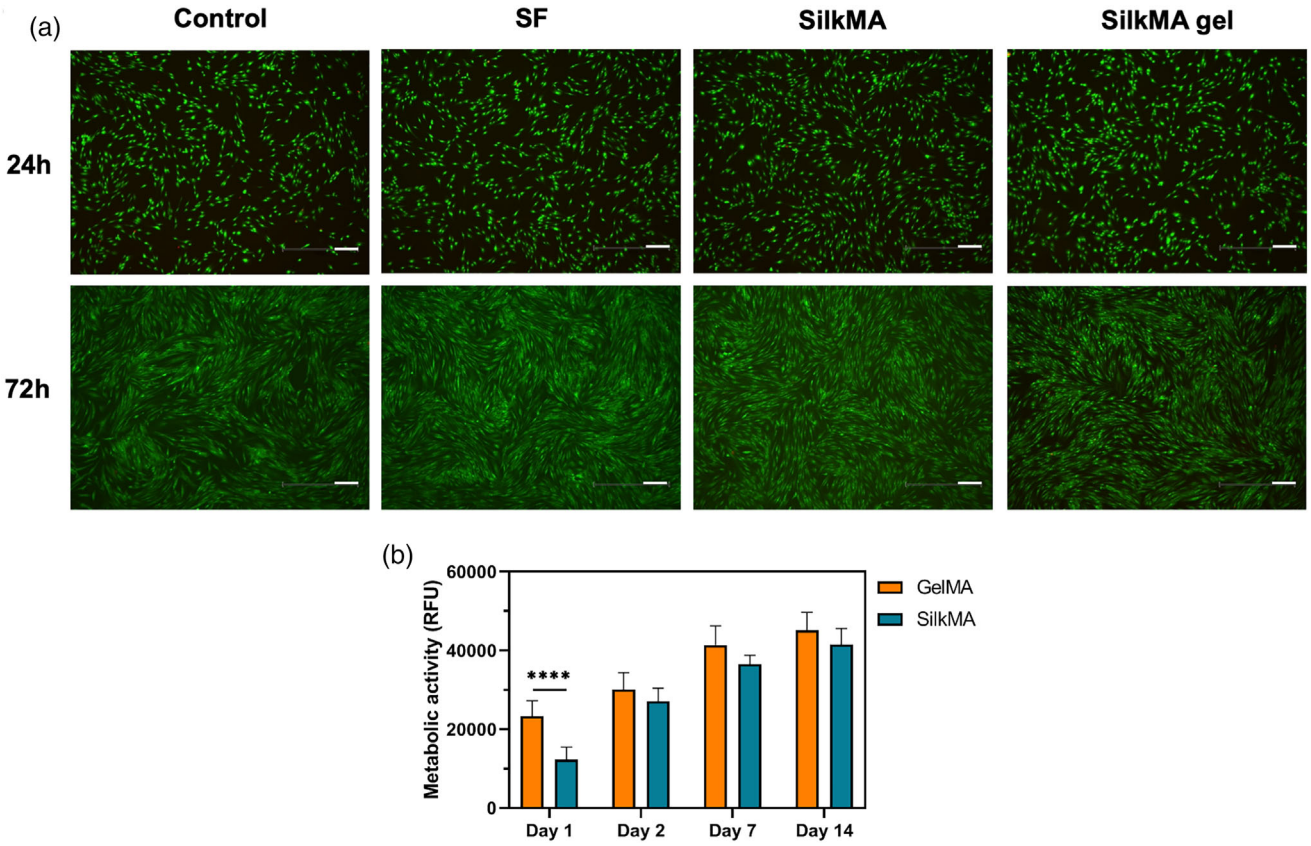

FIGURE 6 Cytocompatibility study: (A) Live/Dead images of HDFs seeded on tissue culture well-plates with media (control) and SF/SilkMA solutions and SilkMA gels in inserts ($n = 3$). Scale bar = 200 μm. (B) Quantification of the metabolic activity of HDFs seeded on SilkMA and GelMA hydrogels by AlamarBlue assay 1, 2, 7, and 14 days after cell seeding ($n = 5$). Data presented as mean value ± *SD* (*****p<.0001)

20% SilkMA hydrogels throughout the experiment (Figure 7C). ZOI varied from 2.6 ± 0.2 cm and 3.0 ± 0.3 cm after 24 h to 1.4 ± 0.1 cm and 1.5 ± 0.1 cm after 72 h for *S.aureus* and *P.aeruginosa*, respectively (Figure 7C). Finally, gentamicin-free SilkMA gels did not inhibit bacterial growth (data not shown).

4 | DISCUSSION

In most cases, vision lost due to corneal-related injuries can be reversed with a corneal transplant. However, currently there is a severe mismatch between supply and demand of cadaveric donor corneal tissue (less than 1:70).[15,16] Despite recent efforts to develop corneal stroma equivalents, the clinical need remains unmet with no products available for routine use.[5,14,15] In this study, we developed an injectable and light-polymerizable SilkMA solution by modifying silk's lysine amino acids with methacrylate groups.

The photosensitive SilkMA solutions have potential to be crosslinked in situ using low UV-A intensities. In 2016, the US Food and Drug Administration (FDA) approved a therapy called corneal crosslinking (CXL) to treat patients with post LASIK/PRK ectasia and progressive corneal thinning (keratoconus). CXL uses UV-A light and riboflavin to stiffen the cornea by inducing covalent bonds between corneal collagen molecules.[42,43] During the treatment, riboflavin is added to the cornea and photoactivated with UV-A light at 365 nm with irradiance of 3 mW/cm^2 for 30 min.[44] In this study, the wavelength and intensity were chosen in agreement with CXL procedure, however instead of irradiating the eye for 30 minutes, the gels set within 5 min with minimal heat production. The impact of polymer concentration on the physical and mechanical properties of the hydrogels was studied. Our results indicate that SilkMA concentration influenced the transparency, swelling characteristics, rheology and mechanical properties of the hydrogels.

The optical functions of the cornea include 80% of the total ocular refractive power, UV light filtering (< 400 nm), and visible light transmission.[38,45] Thus, a successful corneal substitute needs to have similar light transmittance to the native human cornea to replicate its visual acuity. The transmittance results obtained for 15% and 20% SilkMA hydrogels in the visible range match the values reported in the literature for a healthy human cornea (78%–80%).[35,46] Also, the light transmittance spectrum of the human cornea published by Freegard is very similar to the spectra obtained for 15% and 20% SilkMA, with 62% and 90% light transmittance at 400 and 780 nm, respectively.[46]

Another important factor influencing the overall transparency of a hydrogel is the water content. The high hydrophilic character of hydrogels makes them attractive materials for tissue engineering

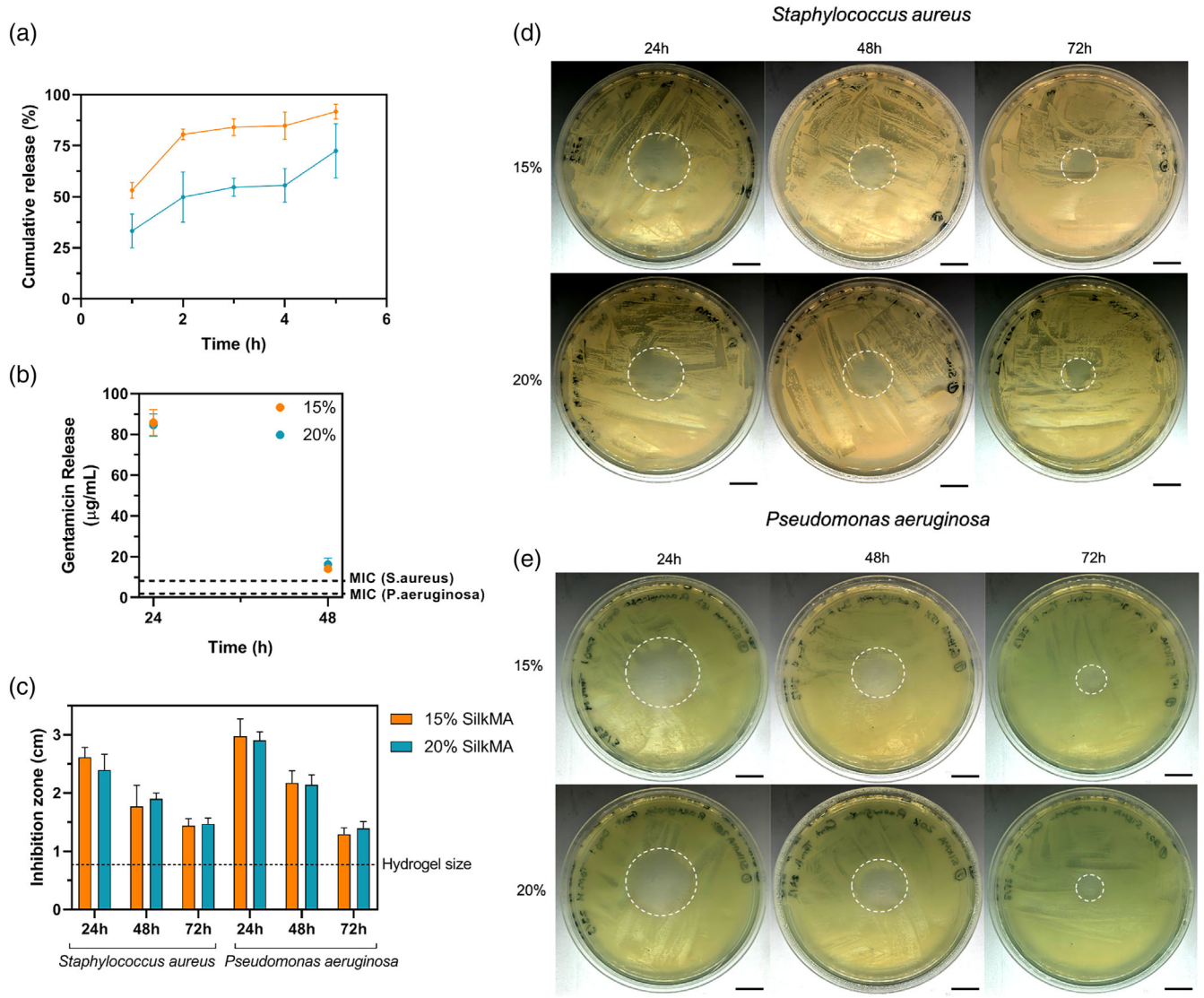

FIGURE 7 In vitro properties of gentamicin-loaded SilkMA hydrogels ($n = 5$): (A) Cumulative gentamicin drug release from SilkMA scaffolds after 1, 2, 3, 4, and 5 h. (B) Gentamicin concentration in the media after 24 and 48 h. Zone of inhibition study ($n = 3$): (C) Average zone of inhibition of SilkMA hydrogels after 24, 48, and 72 h. (D) Staphylococcus aureus, and (E) Pseudomonas aeruginosa. Scale bar = 1.5 cm

applications since the swelling characteristics affect the diffusion and distribution of nutrients, oxygen, and the functionality of encapsulated cells.[1] In vivo variations in water content cause a decrease in corneal transparency due to the changes in the collagen fibrillar spacing and are correlated with several pathologies and diseases (e.g., corneal graft rejection, keratoconus, and Fuchs' dystrophy).[47,48] In this study, all groups showed water content values similar to the human cornea (75%–85%).[45,48] However, as previously reported in the literature, the mass swelling of SilkMA hydrogels decreased with higher polymer concentrations.[10,49–51] An increase in the concentration of photocrosslinkable groups results in a higher crosslinking density, which ultimately creates a tighter hydrogel network and a lower mass swelling ratio. The storage and compressive Young's modulus were directly proportional to the polymer concentration, also indicating a greater crosslinking density. Bryant et al. studied the critical effect of the mass swelling ratio in the formation of a functional ECM.[52] The primary components of cartilage, glycosaminoglycan (GAG) and collagen, were evaluated histologically when varying q from 4.2 to 9.3. Results showed that q has a great effect on cell function. Despite having a similar GAG content in all hydrogels, its distribution depends on the gel properties. In systems with a q of 9.3 (low crosslinking density), GAG molecules were homogenously distributed throughout the gel. On the other hand, in highly crosslinked gels with q values lower than 5.2, GAGs were retained in pericellular regions.[52] In this work, all groups studied presented a q >5.2, with values ranging between 9.8 ± 0.2 and 5.8 ± 0.1 for 15% and 25% SilkMA gels, respectively.[53] Moreover, swelling properties can also affect the overall shape of the material. A successful corneal substitute should have minimal volume change thereby reducing the risk of implant mismatch and imparting stress on the surrounding tissues.[53] All experimental

groups handled well and retained their shape in the swollen state. However, 15% SilkMA hydrogels showed a twofold higher expansion percent than 20% and 25% SilkMA (p <.05).

The success of a corneal substitute is dependent on its ability to sustain epithelial and stromal regeneration. Controlling the degradation rate is paramount since the hydrogel's in vivo degradation should match that of corneal regeneration. Herein, we demonstrate that SilkMA hydrogels can be enzymatically degraded in vitro. A negative correlation between the polymer concentration and the polymer reactivity to enzymatic degradation was observed. At higher cross-linking densities, the enzyme accessibility to the cleavage sites of SF is restricted, decreasing the reactivity of hydrogels to enzymatic degradation.[10] However, the in vitro degradation rate reported in this study is not representative of the ocular in vivo microenvironment. The corneal environment is not as dilute as the conditions used in the swelling and degradation study. In vivo, the surface of the cornea is wetted by the tear film while the overall corneal hydration is controlled by a pumping mechanism in the endothelium.[13] Also, the concentration of collagenase II used in this experiment is not likely to be comparable to the concentrations found in the eye. Nevertheless, our results demonstrate that the chemical modifications on the SF structure did not affect the biodegradability of the polymer. In the future, the actual swelling characteristics, expansion percentage and the rate of in vitro degradation should be studied in an environment more representative of the ocular conditions (e.g., porcine eye model).

Indeed, 25% SilkMA gels exhibited a significantly lower transparency (p <.001) and swelling ratio (p <.0001) than 15% and 20% SilkMA gels. Given the importance of transparency and nutrient transport in the success of a corneal substitute, we chose to move forward with 15 and 20% SilkMA formulations due to their superior transparency and swelling characteristics.

Comprising ~90% of the corneal thickness, the stroma provides the cornea with its mechanical and optical properties due to the lamellar interweaving of collagen fibrils embedded in a hydrated matrix.[54,55] The cornea shows an increase in stiffness associated with age that could be related with a decrease in interfibrillar spacing and an increase in cross-linking between collagen molecules.[56] Despite being essential for the diagnosis of corneal diseases and corneal function maintenance, the rheological and mechanical properties of the cornea are not completely understood and the values reported in the literature span over a large range.[57,58] Hatami-Marbini et al. studied the dynamic shear properties of the corneal stroma using oscillatory experiments. The average G′ and G″ varied from 2 to 8 kPa and 0.3 to 1.2 kPa, respectively. However, hydrogels derived from biopolymers or corneal ECM are reported to have poor mechanical properties compared with the native tissue.[59] In this work, only 20% SilkMA hydrogels exhibited a storage modulus within the above-mentioned range (3.0 ± 0.4 kPa). Despite the lower G″ of SilkMA hydrogels (0.04–0.6 kPa), the overall rheological properties of SilkMA hydrogels are higher than previously investigated light-free collagen-based hydrogels.[2,4] Ferraci et al. synthesized 10%, 15%, and 20% photocurable bovine serum albumin (BSA-MA) with different degrees of substitution (DM = 73%–100%) using UV light (150 mW/cm^2, 6 min). The compressive modulus of 15 and 20% BSA-MA hydrogels with 92 DM% was ~18 and 30 kPa, respectively.[10] In this work, despite using a considerably lower DM% (40%) and intensity (3 mW/cm^2), the compressive modulus of 15% and 20% SilkMA hydrogels was 21 and 79 kPa, respectively. This demonstrates the potential of SilkMA-LAP system for tissue engineering applications, using a relatively low light intensity, hydrogels with excellent mechanical properties can be prepared due to the outstanding mechanical properties of silk proteins.

Moreover, substrate stiffness is reported to influence stem cell differentiation and proliferation.[60,61] Similarly, the hydrogel microstructure also plays an important role in cytocompatibility since porosity and pore size have previously been reported to influence cellular attachment, migration, and tissue ingrowth.[62,63] Although having low porosity (< 80%), which is required for structural properties, both 15 and 20% SilkMA hydrogels showed interconnected and uniform sized pores with an average pore size higher than 50 μm. Murphy et al. investigated the relationship between scaffold pore size and cell activity in bone tissue engineering. Scaffolds with small pores and increased surface area may show higher levels of initial cell attachment, however, the improved cell infiltration provided by scaffolds with larger pore sizes ultimately outweighs this effect.[62,63] In this study, we firstly verified the cytocompatibility of the SF/SilkMA prepolymer solutions and SilkMA hydrogels. Live/dead results showed that the modified and unmodified polymers, photoinitiator, and degradation products did not induce cytotoxicity after 72 h. Then, the hydrogel's ability to support cell attachment was studied. It has been previously reported that silk does not possess cell-adhesion sequences (e.g., RGD) present in other proteins, such as collagen, gelatin, or laminin.[37,64] However, SilkMA hydrogels were shown to support adhesion and proliferation of HDFs for the entire duration of the experiment and the differences between the metabolic activity in SilkMA and GelMA cell-laden hydrogels was only statistically significant at day 1 (p <.0001). The attachment of HDF cells to the SilkMA hydrogels possibly resulted from the hydrophilic nature of the hydrogels and their ability to immobilize adhesive proteins from the serum (e.g., vitronectin and fibrinogen).[10,65] In the future, the viability of cells encapsulated within SilkMA gels should be studied to confirm the suitability of SilkMA as biomaterial and study the impact of photocrosslinking. Importantly, the pore size obtained in this study should not compromise cell viability. Wang et al. encapsulated NIH-3T3 fibroblasts in EY-GelMA hydrogels with similar pore sizes to the SilkMA hydrogels studied here (> 50 μm). The cell viability of 15% and 20% EY-GelMA hydrogels 24 h post cell-seeding was 85.9% and 91.5% (p <.01), respectively. The improved biocompatibility of 20% EY-GelMA gels was attributed to its higher stiffness.[61] In one of the first studies published using SilkMA, Kim et al. demonstrated the suitability of SilkMA bioinks for cell encapsulation. NIH/3T3 fibroblasts were suspended in 10%–30% SilkMA or 10% GelMA (control) and printed using DLP. The authors concluded that cells remained viable regardless of the concentration, with 30% SilkMA gels having a cell proliferation as high as 10% GelMA despite the smaller pore size (≃ 40 μm).[19]

The antibacterial efficiency of gentamicin-loaded SilkMA hydrogels was assessed against *S.aureus* and *P.aeruginosa*, two of the most common causes of ocular infections.[30] Agar diffusion experiments were performed to test the antibacterial properties of 15% and 20% SilkMA hydrogels. Both groups inhibited bacterial growth for 72 h and the ZOIs were not statistically significant between groups throughout the experiment. The fact that the ZOIs for *P.aeruginosa* are higher than *S.aureus* is expected since the MIC for the latter is four times higher.[41] Following the confirmation that the gentamicin-loaded SilkMA hydrogels successfully inhibited bacterial growth, the drug release kinetics and gentamicin concentration in the media were studied. We observed a rapid drug release for both groups with 15% and 20% SilkMA hydrogels releasing 92 ± 4% and 72 ± 13% within 5 h, respectively. In this study, the gentamicin was solely entrapped in the polymer network. Consequently, a quick initial release and a negative correlation between the polymer concentration and the gentamicin drug release rate were expected since loose polymer networks are less able to retain the drug, yielding a quicker release. Importantly, both groups delivered antibiotic concentrations higher than the MIC in the first 48 h which is critical for the successful eradication of a bacterial strain. We believe this discrepancy between the results regarding the antimicrobial testing (agar diffusion test) and the in vitro drug release experiment are due to the different nature of the experiments. When solid agar was used, the drug release profile was slower since only one surface of the gel was in contact with the agar and less liquid volume was available for elution, delaying the drug diffusion. Then, the drug-loaded in the hydrogels was enough to inhibit bacterial growth for 72 h. However, for drug release studies, the hydrogels were soaked in PBS. Since the contact area between the gel and the media was higher, gentamicin was released within a few hours (burst release). However, neither of these conditions is representative of the ocular in vivo microenvironment. In the future, the hydrogels should be tested in an ocular model that considers the presence of the tear film, blinking, and ocular movements. Together, we have demonstrated the photocurable SilkMA hydrogels are able to successfully deliver antimicrobial agents and control their release kinetics to effectively inhibit bacterial growth, ultimately enhancing the potential clinical efficacy of this corneal substitute.

In the present study, we have demonstrated the development of SilkMA hydrogels that replicate the corneal physical properties, in addition to being biodegradable and cytocompatible. The hydrogel biodegradability was tested with collagenase II, an enzyme that can be naturally found in tears.[66] Ideally the material degradation should match de novo tissue formation as cells would secrete enzymes as they migrate. Therefore, we expect the degradation properties of the hydrogels to be linked to cellular integration and tissue formation. Also, gentamicin-loaded SilkMA hydrogels were proven effective against *S.aureus* and *P.aeruginosa*, two of the most common causes of ocular infections, which could improve the overall graft acceptance of this material when compared to the conventional therapies.[30] To our knowledge, this is the first study to assess the utility of SilkMA hydrogels for corneal applications.

The focus of the biological studies carried out in this study was the assessment of SilkMA's cytocompatibility given that the semi-synthetic polymer and the photoinitiator could be a source of cytotoxicity. In the future, the in vitro adhesion, differentiation, and tissue formation of corneal cells within these constructs needs to be investigated. Moreover, due to the difficulty in replicating the complex corneal physiological environment in vitro, such as the ocular movement, blinking, or tear film, in vivo experiments will be required to further understand the therapeutic potential of this material in the repair of corneal injuries. More specifically, the ability of SilkMA hydrogels to fill the corneal defects, support corneal re-epithelization, deliver the optimum release kinetics following surgery and degrade in situ will be addressed.

5 | CONCLUSION

In conclusion, these findings demonstrate the development of an injectable and photocurable SilkMA hydrogel system for corneal regeneration. The material can be either crosslinked in situ within minutes at neutral pH and without heat production using a low-intensity UV light or printed using lithography-based biofabrication techniques. We demonstrated that gentamicin-loaded SilkMA hydrogels are biodegradable, biocompatible, and antimicrobial along with exhibiting optical and mechanical properties similar to the native human cornea. Taken together, these findings demonstrate the considerable potential that SilkMA hydrogels possess as a corneal substitute. To our knowledge, this is the first study to report the utility of photocurable SilkMA hydrogels to promote cornea regeneration.

DATA AVAILABILITY STATEMENT

The data that support the findings of this study are available from the corresponding author upon reasonable request.

ORCID

Kenny Man https://orcid.org/0000-0002-7946-9375
Sophie E. T. Louth https://orcid.org/0000-0003-3065-8201
Sophie C. Cox https://orcid.org/0000-0003-4746-0322
Anita K. Ghag https://orcid.org/0000-0002-6650-3394

REFERENCES

1. Li L, Lu C, Wang L, et al. Gelatin-based photocurable hydrogels for corneal wound repair. *ACS Appl Mater Interfaces*. 2018;10:13283-13292.
2. Chen F, Le P, Fernandes-Cunha GM, Heilshorn SC, Myung D. Bio-orthogonally crosslinked hyaluronate-collagen hydrogel for suture-free corneal defect repair. *Biomaterials*. 2020;255:120176.
3. Kilic Bektas C, Burcu A, Gedikoglu G, Telek HH, Ornek F, Hasirci V. Methacrylated gelatin hydrogels as corneal stroma substitutes: in vivo study. *J Biomater Sci Polym Ed*. 2019;30:1803-1821.
4. Fernandes-Cunha GM, Chen KM, Chen F, et al. In situ-forming collagen hydrogel crosslinked via multi-functional PEG as a matrix therapy for corneal defects. *Sci Rep*. 2020;10:1-13.
5. Duarte Campos DF, Rohde M, Ross M, et al. Corneal bioprinting utilizing collagen-based bioinks and primary human keratocytes. *J Biomed Mater Res - Part A*. 2019;107:1945-1953.

6. Kim H, Park MN, Kim J, Jang J, Kim HK, Cho DW. Characterization of cornea-specific bioink: high transparency, improved in vivo safety. *J Tissue Eng*. 2019;10:204173141882338.
7. Khosravimelal S, Mobaraki M, Eftekhari S, Ahearne M, Seifalian AM, Gholipourmalekabadi M. Hydrogels as emerging materials for cornea wound healing. *Small*. 2021;17:2006335.
8. Cortina M, de la Cruz J. *Keratoprostheses and Artificial Corneas*. Springer-Verlag; 2015.
9. Fagerholm P, Lagali NS, Merrett K, et al. A biosynthetic alternative to human donor tissue for inducing corneal regeneration: 24-month follow-up of a phase 1 clinical study. *Sci Transl Med*. 2010;2:46ra61.
10. Ferracci G, Zhu M, Ibrahim MS, et al. Photocurable albumin methacryloyl hydrogels as a versatile platform for tissue engineering. *ACS Appl Bio Mater*. 2020;3:920-934.
11. Lee HJ, Fernandes-Cunha GM, Myung D. In situ-forming hyaluronic acid hydrogel through visible light-induced thiol-ene reaction. *React Funct Polym*. 2018;131:29-35.
12. Sharifi S, Islam MM, Sharifi H, et al. Tuning gelatin-based hydrogel towards bioadhesive ocular tissue engineering applications. *Bioact Mater*. 2021;6:3947-3961.
13. Koivusalo L, Kauppila M, Samanta S, et al. Tissue adhesive hyaluronic acid hydrogels for sutureless stem cell delivery and regeneration of corneal epithelium and stroma. *Biomaterials*. 2019;225:119516.
14. Isaacson A, Swioklo S, Connon CJ. 3D bioprinting of a corneal stroma equivalent. *Exp Eye Res*. 2018;173:188-193.
15. Zhang B, Xue Q, Li J, et al. 3D bioprinting for artificial cornea: challenges and perspectives. *Med Eng Phys*. 2019;71:68-78.
16. Tonsomboon K, Oyen ML. Composite electrospun gelatin fiber-alginate gel scaffolds for mechanically robust tissue engineered cornea. *J Mech Behav Biomed Mater*. 2013;21:185-194.
17. Sani ES, Lassaletta AD, Wang X, et al. Engineering a highly elastic human protein–based sealant for surgical applications. *Sci Transl Med*. 2017;9(410):eaai7466.
18. Shirzaei Sani E, Kheirkhah A, Rana D, et al. Sutureless repair of corneal injuries using naturally derived bioadhesive hydrogels. *Sci Adv*. 2019;5:eaav1281.
19. Kim SH, Yeon YK, Lee JM, et al. Precisely printable and biocompatible silk fibroin bioink for digital light processing 3D printing. *Nat Commun*. 2018;9:1-14.
20. Mahdavi SS, Abdekhodaie MJ, Kumar H, Mashayekhan S, Baradaran-Rafii A, Kim K. Stereolithography 3D bioprinting method for fabrication of human corneal stroma equivalent. *Ann Biomed Eng*. 2020;48:1955-1970.
21. Kilic Bektas C, Hasirci V. Cell loaded 3D bioprinted GelMA hydrogels for corneal stroma engineering. *Biomater Sci*. 2020;8:438-449.
22. Tabatabai AP, Kaplan DL, Blair DL. Rheology of reconstituted silk fibroin protein gels: the epitome of extreme mechanics. *Soft Matter*. 2015;11:756-761.
23. Costa JB, Silva-Correia J, Oliveira JM, Reis RL. Fast setting silk fibroin bioink for bioprinting of patient-specific memory-shape implants. *Adv Healthc Mater*. 2017;6:1-8.
24. Holland C, Numata K, Rnjak-Kovacina J, Seib FP. The biomedical use of silk: past, present, future. *Adv Healthc Mater*. 2019;8:1800465.
25. Chirila T, Barnard Z, Zainuddin, Harkin DG, Schwab IR, Hirst LW. Bombyx mori silk fibroin membranes as potential substrata for epithelial constructs used in the management of ocular surface disorders. *Tissue Eng A*. 2008;14:1203-1211.
26. Higa K, Takeshima N, Moro F, et al. Porous silk fibroin film as a transparent carrier for cultivated corneal epithelial sheets. *J Biomater Sci Polym Ed*. 2011;22:2261-2276.
27. Barroso IA, Man K, Villapun VM, Cox SS, Ghag AK. Methacrylated silk fibroin hydrogels: pH as a tool to control functionality. *ACS Biomater Sci Eng*. 2021;7(10):4779-4791.
28. Ghobril C, Grinstaff MW. The chemistry and engineering of polymeric hydrogel adhesives for wound closure: a tutorial. *Chem Soc Rev*. 2015;44:1820-1835.
29. Mohammed S, Chouhan G, Anuforom O, et al. Thermosensitive hydrogel as an in situ gelling antimicrobial ocular dressing. *Mater Sci Eng C*. 2017;78:203-209.
30. Khalil IA, Saleh B, Ibrahim DM, et al. Ciprofloxacin-loaded bioadhesive hydrogels for ocular applications. *Biomater Sci*. 2020;8:5196-5209.
31. Veiga AS, Schneider JP. Antimicrobial hydrogels for the treatment of infection. *Biopolymers*. 2013;100:637-644.
32. Cui X, Soliman BG, Alcala-Orozco CR, et al. Rapid Photocrosslinking of silk hydrogels with high cell density and enhanced shape Fidelity. *Adv Healthc Mater*. 2020;9:1-15.
33. Lim KS, Levato R, Costa PF, et al. Bio-resin for high resolution lithography-based biofabrication of complex cell-laden constructs. *Biofabrication*. 2018;10:034101.
34. Bhattacharjee P, Fernández-Pérez J, Ahearne M. Potential for combined delivery of riboflavin and all-trans retinoic acid, from silk fibroin for corneal bioengineering. *Mater Sci Eng C*. 2019;105:110093.
35. Rafat M, Li F, Fagerholm P, et al. PEG-stabilized carbodiimide crosslinked collagen-chitosan hydrogels for corneal tissue engineering. *Biomaterials*. 2008;29:3960-3972.
36. Guimarães CF, Gasperini L, Marques AP, Reis RL. The stiffness of living tissues and its implications for tissue engineering. *Nat Rev Mater*. 2020;5:351-370.
37. Buitrago JO, Patel KD, El-Fiqi A, et al. Silk fibroin/collagen protein hybrid cell-encapsulating hydrogels with tunable gelation and improved physical and biological properties. *Acta Biomater*. 2018;69:218-233.
38. Ahearne M, Fernández-Pérez J, Masterton S, Madden PW, Bhattacharjee P. Designing Scaffolds for Corneal Regeneration. *Adv Funct Mater*. 2020;30:1908996.
39. Lim KS, Schon BS, Mekhileri NV, et al. New visible-light Photoinitiating system for improved print Fidelity in gelatin-based bioinks. *ACS Biomater Sci Eng*. 2016;2:1752-1762.
40. Pepelanova I, Kruppa K, Scheper T, Lavrentieva A. Gelatin-methacryloyl (GelMA) hydrogels with defined degree of functionalization as a versatile toolkit for 3D cell culture and extrusion bioprinting. *Bioengineering*. 2018;5:55.
41. Andrews JM. Determination of minimum inhibitory concentrations. *J Antimicrob Chemother*. 2001;48:5-16.
42. Randleman JB, Khandelwal SS, Hafezi F. Corneal cross-linking. *Surv Ophthalmol*. 2015;60:509-523.
43. Jeng BH. *Advances in Medical and Surgical Cornea*. Springer-Verlag; 2014. doi:10.1007/978-3-662-44888-5
44. Hammer A, Richoz O, Mosquera SA, Tabibian D, Hoogewoud F, Hafezi F. Corneal biomechanical properties at different corneal cross-linking (CXL) irradiances. *Investig Ophthalmol Vis Sci*. 2014;55:2881-2884.
45. Mobaraki M, Abbasi R, Vandchali SO, Ghaffari M, Moztarzadeh F, Mozafari M. Corneal repair and regeneration: current concepts and future directions. *Front Bioeng Biotechnol*. 2019;7:1-20.
46. Freegard TJ. The physical basis of transparency of the normal cornea. *Eye (Lond)*. 1997;11(Pt 4):465-471.
47. Kotecha A. What biomechanical properties of the cornea are relevant for the clinician? *Surv Ophthalmol*. 2007;52:109-114.
48. Taylor ZD, Garritano J, Sung S, et al. THz and mm-wave sensing of corneal tissue water content: in vivo sensing and imaging results. *IEEE Trans Terahertz Sci Technol*. 2015;5:184-196.
49. Kim SH, Chu CC. Synthesis and characterization of dextran-methacrylate hydrogels and structural study by SEM. *J Biomed Mater Res*. 2000;49:517-527.
50. Hoch E, Hirth T, Tovar GEM, Borchers K. Chemical tailoring of gelatin to adjust its chemical and physical properties for functional bioprinting. *J Mater Chem B*. 2013;1:5675-5685.

51. Hoch E, Schuh C, Hirth T, Tovar GEM, Borchers K. Stiff gelatin hydrogels can be photo-chemically synthesized from low viscous gelatin solutions using molecularly functionalized gelatin with a high degree of methacrylation. *J Mater Sci Mater Med*. 2012;23:2607-2617.
52. Bryant JS, Anseth SK. Hydrogel properties influence ECM production by chondrocytes photoencapsulated in poly(ethylene glycol) hydrogels. *J Biomed Mater Res*. 2002;59:63-72.
53. Assmann A, Vegh A, Ghasemi-Rad M, et al. A highly adhesive and naturally derived sealant. *Biomaterials*. 2017;140:115-127.
54. Frederick S, Brightbill MD, McDonnell PJ, McGhee CNJ, Farjo AA. *Corneal Surgery: Theory Technique and Tissue*. Mosby; 2009.
55. Brunette I, Roberts CJ, Vidal F, et al. Alternatives to eye bank native tissue for corneal stromal replacement. *Prog Retin Eye Res*. 2017;59:97-130.
56. Elsheikh A, Wang D, Brown M, Rama P, Campanelli M, Pye D. Assessment of corneal biomechanical properties and their variation with age. *Curr Eye Res*. 2007;32:11-19.
57. Hatami-Marbini H, Etebu E. Rate dependent biomechanical properties of corneal stroma in unconfined compression. *Biorheology*. 2013;50:133-147.
58. Qin X, Tian L, Zhang H, Chen X, Li L. Evaluation of corneal elastic modulus based on corneal visualization Scheimpflug technology. *Biomed Eng Online*. 2019;18:1-16.
59. Ahearne M, Coyle A. Application of UVA-riboflavin crosslinking to enhance the mechanical properties of extracellular matrix derived hydrogels. *J Mech Behav Biomed Mater*. 2016;54:259-267.
60. Engler AJ, Sen S, Sweeney HL, Discher DE. Matrix elasticity directs stem cell lineage specification. *Cell*. 2006;126:677-689.
61. Wang Z, Kumar H, Tian Z, et al. Visible light Photoinitiation of cell-adhesive gelatin Methacryloyl hydrogels for Stereolithography 3D bioprinting. *ACS Appl Mater Interfaces*. 2018;10:26859-26869.
62. Murphy CM, Haugh MG, O'Brien FJ. The effect of mean pore size on cell attachment, proliferation and migration in collagen-glycosaminoglycan scaffolds for bone tissue engineering. *Biomaterials*. 2010;31:461-466.
63. Murphy CM, O'Brien FJ. Understanding the effect of mean pore size on cell activity in collagen-glycosaminoglycan scaffolds. *Cell Adhes Migr*. 2010;4:377-381.
64. Silva SS, Popa EG, Gomes ME, et al. Silk hydrogels from non-mulberry and mulberry silkworm cocoons processed with ionic liquids. *Acta Biomater*. 2013;9:8972-8982.
65. Fleischer S, Shapira A, Regev O, Nseir N, Zussman E, Dvir T. Albumin fiber scaffolds for engineering functional cardiac tissues. *Biotechnol Bioeng*. 2014;111:1246-1257.
66. Sariri R, Ghafoori H. Tear proteins in health, disease, and contact lens wear. *Biochemistry*. 2008;73:381-392.

SUPPORTING INFORMATION

Additional supporting information may be found in the online version of the article at the publisher's website.

How to cite this article: Barroso IA, Man K, Hall TJ, et al. Photocurable antimicrobial silk-based hydrogels for corneal repair. *J Biomed Mater Res*. 2022;110(7):1401-1415. doi:10.1002/jbm.a.37381